Preionization for Collisionless Shock Wave Experiments by Means of Photoionization

M. Keilhacker, F. Pecorella[+], and G.C. Vlases[++]

IPP 1/99 December 1969

INSTITUT FÜR PLASMAPHYSIK

GARCHING BEI MÜNCHEN

INSTITUT FÜR PLASMAPHYSIK

GARCHING BEI MÜNCHEN

Preionization for Collisionless Shock Wave Experiments by Means of Photoionization

M. Keilhacker, F. Pecorella[+], and G.C. Vlases[++]

IPP 1/99 December 1969

[+] Present Address: Laboratori Gas Ionizzati, Frascati (Roma), Italy

[++] Present Address: University of Washington, Seattle, USA

Die nachstehende Arbeit wurde im Rahmen des Vertrages zwischen dem Institut für Plasmaphysik GmbH und der Europäischen Atomgemeinschaft über die Zusammenarbeit auf dem Gebiete der Plasmaphysik durchgeführt.

IPP 1/99

M. Keilhacker
F. Pecorella
G.C. Vlases

Preionization for Collisionless Shock Wave Experiments by Means of Photoionization.

December 1969 (in English)

Abstract

Strong ultraviolet radiation emitted from a dynamically filled linear z-pinch in xenon is used to ionize low density molecular hydrogen and the noble gases. The technique can be used to produce an initial plasma with electron densities of 10^{12} - 10^{14} cm^{-3} suitable for collisionless shock wave experiments. The degree of ionization which can be achieved at the center of a 150 cm long test chamber having one light source at each end ranges at 1 mtorr filling pressure from 20 % in H_2 to 63 % in xenon. The plasma is relatively homogeneous, current and impurity free, and has an electron temperature of about 1 eV.

In order to compare the efficiency of hydrogen and xenon in the light source in transforming energy originally stored in the capacitor bank into photon energy in the necessary wavelength region, the absorption of energy from the capactitor bank by the z-pinch and the radiation emitted by the pinched gas are estimated for both gases. The calculation shows, in agreement with the experimental results, that with xenon as the source gas a much higher ionization rate as with hydrogen is produced. Furthermore, it appears that the peak density reached in these experiments is limited by the energy available in the driving capacitor bank.

To get a picture of the space-time dependence of density, electron temperature, and ion temperature in the photoionized gas, the relevant set of coupled differential equations is solved numerically. The calculations show that for conditions resembling those of the experiment the energy equipartition time between electrons and ions can be made shorter than the times for radial diffusion and heat conduction by superimposing an axial magnetic field on the order of 100 Gauss.

Table of Contents

I. Introduction

In this paper we describe a technique for producing a low density ($n_e \approx 10^{12} - 10^{14} cm^{-3}$) highly ionized plasma by means of photoionization. The motivation for this work comes from collisionless shock wave experiments, in which attainment of a clean, uniform initial plasma presents a major problem. The technique described here, however, is not restricted in application to such problems, and in fact is capable of providing an initial plasma for a great variety of experiments.

Most of the collisionless shock wave experiments reported to date rely on high currents in the discharge chamber to produce the initial plasma, either by direct coupling, such as in Z-pinches[1] and inverse pinches[2], or by inductive coupling, such as in θ-pinches [3-6]. The plasma is heated by a combination of shock wave produced viscous dissipation and Ohmic heating.

There are several difficulties inherent in current-induced preionization. Large inhomogeneities in the plasma density and the applied magnetic field are produced by the Lorentz forces, impurities are often a problem (especially in the direct-coupled devices), and ionization becomes more difficult to achieve at the lower pressures[7]. Unwanted residual currents flow in the plasma for long times. The preionization process is often relatively slow, with a time scale of tens or hundreds of microseconds, to allow time for re-establishment of uniform conditions; this compounds the problems of impurities and plasma losses. Finally, conditions achieved depend strongly on the initial magnetic field strength.

In order to overcome as many of these difficulties as possible, work on a photoionization technique was begun at the Institut für Plasmaphysik by G.Hofmann[8,9]. Many of the experimental techniques reported in this paper are a carry over and extension of his ideas. More recent results have been

reported by Pecorella and Vlases[10].

Creation of an initial plasma by means of photoionization has many potential advantages. The initial plasma is quiescent, homogeneous, current free, and impurity free. The method works very well at lower filling densities where other methods fail and produces a plasma whose properties are initially independent of the magnitude and direction of the applied magnetic field. There are also drawbacks to the method, relating chiefly to the difficulty of producing a sufficiently strong photoionizing source, and to the somewhat peculiar nature of the plasma so produced.

Following an explanation of the technique used to preionize a plasma by means of photoionization (Section II), the experimental results are presented (Section III). In Section IV we first discuss the photoionizing light source from the standpoint of optimizing its performance, after which we develop a simple model for the production and decay of the photoionized plasma. The conclusions reached are stated in Section V.

II. Experimental Technique

In order to photoionize molecular hydrogen or the noble gases, a light source that produces a strong flux of photons with wavelengths lying between roughly 5oo Å and 11oo Å is required. Figure 1 shows photoionization cross sections for the gases studied, as taken from Marr[11].

A high voltage (12o kV) linear pinch driven by a single o.84 μF capacitor is used as the light source. Since no windows exist in the necessary wavelength region of the spectrum, the light source must be located within the same vacuum vessel as the gas to be preionized (test gas).

In the present experiments one such light source is connected to the end of a cylindrical glass pipe 15 cm in diameter by 15o cm in length. The pinch chamber is made from a 15 cm (nominal) diameter glass cross with copper electrodes inserted, as shown schematically in Figure 2 a. In order to reduce impurities from ablation products all components are of metal or glass. The return leads (not shown) are fitted as closely as possible to the glass vessel to reduce inductance and enhance pinch formation and stability.

In future applications two sources will be used (Figure 2b), one at each end. The test chamber diameter may be made larger without reducing the degree of ionization achieved at a given filling pressure.

Optimum ionizing radiation is achieved by using one of the heavier noble gases (particularly Xe) at a relatively high filling pressure as the source gas. The test chamber is first filled to the desired pressure, typically 1 to 1o mTorr. The source gas is then admitted to the chamber through a hole in the upper electrode by means of a fast-acting valve, whose

design and testingare described in reference 12). After a certain time the pinch current is initiated, producing the photoionizing radiation. Gas from the light source eventually reaches the center of the test chamber, but this happens only on a time scale that is long (> loo μsec) compared to the duration of the collisionless shock experiments conducted in the test chamber following the creation of the initial plasma.

While the photoionizing reactions which produce the plasma in the test chamber are independent of magnetic field, the subsequent evolution of the plasma is not. For this reason provision was made to establish a magnetic field over a portion of the length of the test chamber. This field is produced by a four-coil corrected system[13] whose axis coincides with that of the tube. The resulting field is quasi-stationary on the time scale of the plasma decay, has a maximum strength of 2.5 kG, and is approximately homogeneous in a region 36 cm long centered at a point loo cm from the light source.

A variety of diagnostic techniques is employed. An image converter camera is used to take both streak and framing pictures of the pinch. The electron density of the test gas is measured as a function of time at a particular axial location by an 8 mm microwave interferometer. The electron temperature is measured by laser scattering techniques using a 600 MW, 12 nsec pulsed ruby laser and a narrow band-width interference filter[14]. This measurement also gives an independent check on the electron density. The composition of the plasma is determined with a mass spectrometer.

III. Experimental Results

1) Maximum Attainable Degree of Ionization

For the density of electrons n_e produced by photoionization at distance z from the light source (approximated as a point source) with spectral light flux $s(t,\nu)$ the following equation holds[8]:

$$\frac{\partial n_e(t,z)}{\partial t} = \frac{1}{4\pi z^2} \int_{\nu_0}^{\infty} \frac{\sigma(\nu)\, n_n(t,z)\, s(t,\nu)\, e^{-\sigma(\nu) n_n(t,z) z}\, d\nu}{h\nu} \qquad (1)$$

where $\sigma(\nu)$ = cross-section for photoionization, $n_n(t,z) = n_n(o) - n_e(t,z)$ = density of neutrals, $n_n(o)$ = density of neutrals at time $t = 0$, ν_0 = lower frequency limit for photoionization. It follows from equation (1) that the electron density decreases strongly with distance from the light source and that in order to reduce the axial variation of density it is advantageous to use two light sources, one at each end of the discharge tube, as shown in Figure 2b. The electron density then has a minimum in the median plane and increases towards each light source. Equation (1) also shows that the degree of ionization

$$\alpha(t) = \frac{n_e(t)}{n_n(t) + n_e(t)} \approx \frac{n_e(t)}{n_n(o)}$$

obtainable with a given light source increases with decreasing neutral particle density until the gas is optically thin, i.e. $\sigma\, n_n\, z \ll 1$, and then remains constant, indicating that

photoionization is particularly suited to the preionization of gases at low pressures. For z = 100 cm, $\sigma n_n z = 0.125$ for H_2 at 3 mTorr and 0.04 at 1 mTorr at a wavelength of 800 Å, where σ attains its maximum value.

Assuming the gas is optically thin, the following equation for the degree of ionization can be derived from equation (1)

$$\alpha(t,z) = 1 - \exp\left\{-\frac{1}{4\pi z^2} \int_0^t \int_{\nu_0}^{\infty} \frac{\sigma(\nu)\, s(t,\nu)\, d\nu\, dt}{h\nu}\right\} \qquad (2)$$

In evaluating the electron density from the observed microwave interferometer fringe shifts it is assumed that the radial density distribution is homogeneous (this assumption is correct for the first few μsec, c.f. section IV B). The maximum degree of ionization α_{max} is reached at a few μsec after initiation of the pinch (c.f. Figure 5).

The maximum degree of ionization attained depends on the type and amount of source gas in the pinch chamber, while the amount in turn depends on the delay time between opening of the inlet valve and initiation of the discharge. A reduced time scale $\tau = t(m_i/m_{H_2})^{-1/2}$ is used to compare the different source gases, where m_{H_2} and m_i are the masses of a hydrogen molecule and of the gas in question, respectively. The optimum delay time is found to be about $90(m_i/m_{H_2})^{1/2}$ microseconds (Figure 3) which corresponds roughly to the time required for a molecule to go halfway from the gas inlet to the lower electrode at its room temperature speed of sound. At shorter delay times α_{max} decreases to the value obtained without opening the pulsed valve at all, in which case the z-discharge forms a sliding

spark along the wall of the z-pinch tube. All results described in the following section have been obtained at the optimum delay times.

Figure 4 shows α_{max} as a function of the capacitor voltage U_o for xenon in the z-pinch and different pressures of the hydrogen and argon gas to be ionized. The degree of ionization attained with xenon is approximately proportional to the energy stored in the capacitor in the range from 100 to 120 kV; when hydrogen was used in the z-pinch a weaker dependence was found. It can also be seen from Figure 4 that the degree of ionization attainable with a given light source increases with decreasing filling pressure of the test gas, as was expected from equation (1) for the range of pressures investigated.

While H_2 and deuterium are the most often used gases in pulsed plasma experiments, it is nevertheless interesting to investigate other gases as well. Figure 1 indicates that, with a given light source, an increase in α_{max} should be observed with the noble gases due to their larger photoionization cross sections. Experiments were therfore carried out using argon and xenon as the test gas, as well as H_2. Table I summarizes the degree of ionization that could be achieved with various test gases in the center of a 150 cm discharge tube, if a double-ended xenon source such as shown in Figure 2b were used. The values listed are extrapolated from measurements of the electron density obtained with a single source at $z = 100$ cm using equation (2).

2) Time - variation of Density and Temperature in the Photoionized Plasma

Figure 5 shows some typical examples of the time-variation of electron density n_e produced by photoionization in hydrogen and argon.

The maximum density is reached at a time varying from about 1.5 to 4 μsec after initiation of the pinch, depending on the test gas. As will be shown in section IV A 2, a further build-up of electron density was probably limited by the energy available in the capacitor bank. After reaching a maximum the density decays nearly exponentially, indicating that the main loss is due to ambipolar diffusion to the walls. This is supported by the result that the superposition of axial magnetic fields greatly reduces the decay.

Figure 6 shows the electron temperature T_e on the tube axis as a function of time after initiation of the pinch for a 6 mTorr hydrogen plasma. The rapid decrease in T_e at early times is probably due to heat conduction to the walls and particularly to an exchange of energy with the cold ions which are heated only by collisions with the electrons. The temperature equipartition time is a few μsec in the hydrogen plasma for the present conditions. A model which qualitatively describes the observed time-variation of density and electron temperature and its dependence on superposed axial magnetic fields is given in section IV B 2.

3) Mass Spectrometric Analysis of the Test Gas

In the case of hydrogen as the test gas the mass composition of the photoionized plasma was investigated with a mass spectrometer [15] that consisted essentially of an electrostatic energy analyzer, a particle detector and collector electrodes that accelerate the ions to the energy at which the analyzer is adjusted. The mass of the ions is then determined from their time of flight, their relative intensity from the amplitude of the detector signal. The results, though still rather vague due to ambiguities in the mass dependence of ion extraction and

detection sensitivity, are as follows[16]: The photoionization of H_2 by the radiant flux first results in about 90 % H_2^+ and 10 % H^+. While the intensity of H_2^+ peaks at 1 to 2 µsec the maximum of H^+ is somewhat later. At a filling pressure of 10 mtorr H_2, H_3^+ builds up during the decay phase of H_2^+ (by collisional reactions) and reaches about 10 %, while at 1 mtorr H_2 the amount of H_3^+ is negligible. Superposition of an axial magnetic field of a few hundred Gauss increases the ratio of H^+ to H_2^+, especially at low filling pressures (at 1 mtorr H_2 by about a factor 4). These results are qualitatively the same for H_2 or Xe in the Z-pinch.

In the case of Ne, Ar and Kr as the test gas (Xe in the z-pinch) the ions are singly ionized with a negligible number of multiply ionized species.

IV. Discussion of Results

A. The Z-Pinch Radiation Source

1) Absorption of Energy from the Capacitor

The results discussed above are considerably better than those achieved earlier by Hofmann, using lithium[8] and hydrogen[9] as source gases. In this section we discuss qualitatively the reasons for this and implications for further improvements.

The function of the source gas is to transform energy originally stored in the capacitor bank into photon energy in the necessary wavelength region in as efficient a manner as possible. Energy is deposited in the source gas both by means of Joule heating and viscous heating arising from the shock wave which bounds the imploding sheath. Assume that the pinch dynamics can be satisfactorily described by snowplow theory. Then the kinetic energy per particle behind the incident shock can be shown to scale as $m_i^{1/2}$ for the case where the shock transit time remains less than the 1/4 cycle time of the drive bank, and with a weaker (positive) power of m_i when the inequality is reversed. For our experimental conditions, the ratio of shock wave invested kinetic energy for xenon as compared to hydrogen is 3. The shock wave also invests the gas in the sheath with a thermal energy approximately equal to its directed energy[17]; the directed energy is converted to thermal when the shock reflects from the axis. In general then, heavy gases (e.g. xenon) are more efficient at absorbing energy by shock heating with a given capacitor bank than is hydrogen.

Although the energy in the pinched gas is much higher with xenon than hydrogen, the temperature of xenon is much lower because of the occurrence of multiple ionization.

An approximate calculation has been made of conditions in the pinch column after reflection of the incident shock. This calculation uses plane shock real gas jump conditions[17] based on shock speeds observed with the streak camera. Tabulated values of the Saha equation[18] are used up to a temperature of about 40,000°K and extrapolations are made past this point. The results show that the temperature of the xenon is in the range of 4 to 6 eV with most of the ions being four to six times ionized. The total energy deposited in the pinched gas by shock heating is 2 to 3 kJ. Details are given in Appendix I of this report. As streak photographs show, the pinch is quite stable and remains intact for several microseconds during which time Joule heating continues to deposit energy in the gas while it is being lost by radiation. The relatively low temperature of the xenon results in a high resistivity and hence more efficient energy transfer by Joule heating as well. The same calculation for hydrogen shows that the imploding shock is sufficiently strong to completely ionize the gas, so that upon reflection the temperature shoots up strongly to 50 eV or more. At these temperatures the plasma resistivity is low and the energy deposition rate from Joule heating is correspondingly diminished over that for xenon. As streak photographs show, the pinch is much less stable and breaks up almost immediately after the first implosion.

2) Emission of Radiation

The ionizing efficiency of the radiation depends both on the total power radiated and on the spectral distribution of radiation. The values of $\partial n_e / \partial t$ measured in the test gas indicate the source to be about an order of magnitude stronger initially with xenon than with hydrogen. However $\partial n_e / \partial t$ levels off sharply in the case of xenon after the imploding sheath reaches minimum diameter, which happens (in xenon) after

approximately 3 half-cycles of the capacitor. With hydrogen as the source, the electron density rises much more slowly for a longer time, but reaches a peak value of only about half that attained with xenon.

The emission of a sphere of uniform hydrogen plasma has been calculated by Hofmann and Pecorella[19], who solved the radiative transfer problem and took into account all the relevant free-free, free-bound, and bound-bound transitions in computing the emission coefficient. In their work, the principal contribution to the flux comes from free-bound transitions (radiative recombination) at temperatures of a few electron volts, and from free-free transitions (Bremsstrahlung) at temperatures of tens of electron volts. Using results inferred from these calculations, a comparison between a xenon pinch column of 1 cm diameter at low temperature and a hydrogen pinch column of the same diameter at high temperature, consistent with the conditions of our experiment based on the calculations described above, can be made. In both cases, the density is assumed to be 10^{18} cm^{-3}. For hydrogen at temperatures of 20 to 60 eV, only Bremsstrahlung is taken into account. For xenon, at a few eV, the largest contribution to the emission coefficient comes from radiative recombination, and can be calculated from Griem's formula[20]. The calculation is based on the following assumptions:

(a) Saha equilibrium at the assumed n_e and T_e
(b) All ions in the ground state
(c) A mean value of the angular momentum quantum number taken for all levels is the given principal quantum number
(d) Recombination only to the ground state and the 1st excited levels
(e) Bremsstrahlung small compared to radiative recombination.

Details of the calculations are given in Appendix II of this report. They show that a 1 cm column of xenon is optically thick at a density of $10^{18}cm^{-3}$ and a temperature of 1 eV, but becomes thin at this density above T_e = 2 eV. At $n_e = 10^{19}cm^{-3}$, the plasma is thick at 2 eV, but it is unlikely that our plasma is that dense, since this would require an energy content in the column that is too large for the given capacitor bank. The hydrogen is, of course, thin at $10^{18}cm^{-3}$ and 50 eV.

Since the 1 cm columns of xenon at a few eV, and hydrogen at 40 to 60 eV are both thin at $10^{18}cm^{-3}$ the relative degree of ionization produced per unit time by the two sources can be calculated from

$$\frac{\partial \alpha}{\partial t} \sim \int_{\nu_0}^{\infty} \frac{\sigma \, \varepsilon \, d\nu}{h \nu}$$

which follows from eq.(1) with $s(t, \nu) \sim \varepsilon$, ε being the emission coefficient. The results of this calculation are shown in Figure 7, from which it can be seen that a xenon column at a few eV produces a roughly 2 orders of magnitude higher ionization rate than hydrogen of the same density and geometry, with a temperature of 40 - 60 eV. This is in agreement with the experimental findings. As a side remark we note that the free bound emission coefficient is proportional to the 4th power of the ionic charge, so that triply ionized xenon, as we have in our pinch, has a relatively high emission coefficient.

There remains to be discussed the question of why the photoionizing flux decreases rapidly, i.e., why the build-up of ionization in the test gas ceases, at about the time the xenon pinch reaches minimum diameter. Three

possibilities suggest themselves. First, "loss processes" in the test gas (recombination, diffusion to the walls, etc) could prevent further increase in n_e. This possibility can be ruled out, as shown by the analysis in section IV B 2. Secondly, if the source radiates as a black body, its size, and hence total radiated power, decreases as the sheath implodes and reaches a minimum which it maintains for a relatively long time due to the greater stability of pinches in heavy gases. While this decrease in source size cannot be completely discounted as a factor in explaining n_e (t) the calculations discussed above indicate that the source is probably not a black body. Finally, it is possible that the pinch simply runs out of energy at the time the maximum density is observed. A rough calculation based on equation (1) using measured values of $\partial n_e / \partial t$ and simplifying the integral by using mean values shows that initially the power radiated below the photoionization cut off limit (803 Å for H_2) is about 5×10^8 watts. This should be compared with an average power level for the discharging capacitor of 4×10^8 watts (6 kJ dumped in 10 μsec). Thus it appears that the peak density reached in our experiments is limited by the energy available in the driving capacitor bank.

In view of the foregoing remarks it may be possible to further improve the source by a number of methods. The most obvious is to increase the energy of the capacitor bank. This should be effective since the temperature of the xenon column is very well regulated by the multiple ionization so that the radiation will continue to be in the proper wavelength region. In addition the time scale for loss of photoionized plasma by diffusion and conduction in a magnetized cylindrical colume is considerably longer than the present source duration, so that losses would not limit $n_{e\ max}$ for a somewhat longer lived source. It may also be possible to increase the efficiency of the light source by using mirrors to reflect some of the radiation into the rest section that would otherwise be lost. The best available material, zinc sulfide, reflects about 10 % of the radiation incident upon

it in the range from 500 to 1000 Å [21], which could provide a large improvement in α_{max} if the test chamber could be coated.

It is entirely possible that configurations other than a linear pinch may be better light sources. In preliminary experiments we have substituted a small "plasma focus" for the pinch, using the same capacitor and pulsed gas filling system. The results show that the same degree of ionization is attained as with the z-pinch ($n_{e\ max}$ is probably again energy-limited), but that the maximum is reached in about 1 μsec, rather than 3 or 4 μsec.

B. The Preionized Plasma

1) Products of the Photoionizing Reactions

When the noble gases are photoionized by our light source, the products of the reaction are singly charged ions and electrons, e.g. $A + h\nu \rightarrow A^+ + e$. The source apparently produces very little radiant flux in the wavelength range required for second ionization of the noble gases, i.e. below roughly 500 Å. Although this statement has not been substantiated by direct measurement of the spectrum of the source, it can be inferred by the fact that experiments using He (1st ionization potential = 25.4 eV) as the test gas showed an extremely low degree of ionization.

When H_2 is photoionized, the situation is much more complicated. As discussed by Hofmann [8], the dominant reaction is [22]

$$H_2 + h\nu \longrightarrow H_2^+ + e$$

Direct production of H^+ and direct photodissociation of H_2 into 2H are much less likely[11]. Following the initial reaction which forms H_2^+, a number of secondary reactions involving both photon-particle and particle-particle processes may occur. The subsequent evolution of the plasma composition has not yet been studied theoretically. In the following section, which deals with diffusion and conduction losses, the composition has been assumed constant over the time scales of interest. From the mass spectrometric results discussed above, however, it appears that the production of H^+ and H_3^+ by collisions of H_2 with H_2^+ may be important.

2) Time Evolution of the Test Gas

The variation of electron density $n_e(r,t)$ in the pre-ionized plasma can be expressed by the equation

$$\frac{\partial n_e}{\partial t} = S(t) + D_a \nabla^2 n_e + n_e n_n R - n_e^2 Q \qquad (3)$$

where $S(t)$ stands for the right hand side of equation (1) and describes the build-up of electron density by photoionization, the third term represents collisional ionization by electrons and the second and last terms the decay of electron density due to ambipolar diffusion and volume recombination, respectively. $D_a = D_a(T_e, T_i, n_n, B_o)$ is the ambipolar diffusion coefficient, $R = R(T_e, n_e)$ and $Q = Q(T_e, n_e)$ are the rate coefficients for ionization and recombination, which for an optically thin hydrogen plasma have been calculated by Bates et al.[23]. An order of magnitude estimate shows that in H_2 for the measured electron temperatures the last two terms of equation (3) are small compared to the measured density change (collisisional ionization would become important for $T_e > 2$ eV and recombination for $T_e < 0.2$ eV) and can be

ignored. Equation (3) then reduces to

$$\frac{\partial n_e}{\partial t} = S(t) + D_a \nabla^2 n_e \qquad (4)$$

S(t) is not known, but for the first 2 μsec it can be determined from the measured rise in electron density and can be approximated by a constant ($S(t) = S$ for $0 < t < 2$ μsec). An average (constant) value of D_a can be computed from the measured decay curves, which are nearly exponential, or computed directly from assumed (constant) temperatures for the ions ($300^{\circ}K$) and electrons (1eV). Equation (4) can be solved analytically[24] for D_a = constant. The solution indicates that the radial distribution of plasma density should be flat to within 2 cm of the wall during the duration of the source. Thus, the maximum α obtained in these experiments is limited by energy available in the capacitor bank, and not by loss of electrons due to diffusion or volume recombination.

The measurements of T_e indicate large temperature changes on the time scale of the decay, invalidating the assumption of constant diffusion coefficient invoked above. Thus a more realistic model has been developed to take into account the changes in ion and electron temperatures due to heat conduction and energy equipartitioning. On the other hand the problem has been simplified by setting $S(t) = 0$, i.e. the model starts when the photoionizing reactions have stopped. The plasma is assumed to be an infinitely long cylinder of radius R with a rectangular distribution of temperature and density at $t = 0$. The problem is described by a continuity equation for electrons, two

energy equations, and a macroscopic velocity given by the ambipolar diffusion approximation. The equations[+)] for this model[++)] are [26]:

$$\frac{\partial n_e}{\partial t} = -v_r \frac{\partial n_e}{\partial r} - n_e \frac{1}{r} \frac{\partial}{\partial r}(r v_r) \tag{5}$$

$$\frac{\partial (kT_e)}{\partial t} = -v_r \frac{\partial (kT_e)}{\partial r} - \frac{2}{3}(kT_e) \frac{1}{r} \frac{\partial}{\partial r}(r v_r) + \frac{2}{3} \frac{1}{n_e r} \frac{\partial}{\partial r}\left(r \varkappa_e \frac{\partial T_e}{\partial r}\right) - \frac{(kT_e)-(kT_i)}{t_{eq}} \tag{6}$$

$$\frac{\partial (kT_i)}{\partial t} = -v_r \frac{\partial (kT_i)}{\partial r} - \frac{2}{3}(kT_i) \frac{1}{r} \frac{\partial}{\partial r}(r v_r) + \frac{2}{3} \frac{1}{n_e r} \frac{\partial}{\partial r}\left(r \varkappa_i \frac{\partial T_i}{\partial r}\right) + \frac{(kT_e)-(kT_i)}{t_{eq}} \tag{7}$$

$$n_e v_r = -D_a \frac{\partial n_e}{\partial r} \tag{8}$$

The two last terms on the right hand side of equations (6) and (7) represent the temperature changes due to heat conduction and energy equipartitioning. The boundary conditions for each of the equations are

+) All formulas are written in c.g.s. units.

++) Meanwhile the model has been extended to include collisional excitation, ionization, and recombination [29].

$$\frac{\partial A}{\partial r} = 0 \quad \text{for} \quad r = 0$$

$$A = A_R \quad \text{for} \quad r = R$$

$$A = A(0) \quad \text{for} \quad t = 0$$

where A stands for n_e, T_e and T_i, respectively.

For the ambipolar diffusion coefficient D_a in a magnetic field the following expression is used (see for example[25]):

$$D_a = \frac{\frac{kT_i}{m_i}\left(1 + \frac{T_e}{T_n}\right) t_{cn}}{1 + \omega_e\, \omega_i\, t_{cn}^2} \tag{9}$$

where $\omega_{e,i} = \frac{e B_o}{m_{e,i}\, c}$ is the cyclotron frequency for electrons and ions (e = charge of electron, c = speed of light, $m_{e,i}$ = electron and ion mass respectively, B_o = axial magnetic field), T_n the neutral gas temperature and t_{cn} the collision time between electrons and neutrals. For collisions of electrons with H_2, we have[25] $(t_{cn})^{-1} = 5.93 \times 10^9 \times p(\text{Torr})$.

For the coefficients of heat conduction by electrons and ions, κ_e and κ_i, the formulas given in reference 26) for a fully ionized plasma are used (the corrections for the neutral gas component are negligible for our conditions):

$$\kappa_e = 1.34 \frac{k}{m_e}\, n_e (kT_e) \frac{t_{ce}}{(1 + 0.55\, \omega_e^2\, t_{ce}^2)} \tag{10}$$

$$\kappa_i = \frac{6.25}{\psi} \cdot \frac{k}{m_i}\, n_e (kT_i) \frac{t_{ci}}{\left(1 + \frac{6.25}{\psi^2}\, \omega_i^2\, t_{ci}^2\right)} \tag{11}$$

where $\psi = 1.41 + 7.5 \left(\frac{m_e}{m_i}\right)^{1/2} \left(\frac{T_i}{T_e}\right)^{3/2}$

t_{ce} and t_{ci} are the self-collision times for electrons and ions, and t_{eq} (last term in equation (6) and (7)) is the temperature equipartition time for electrons and ions. For these times, which are defined and calculated in reference 27) the following formulas hold

$$t_{ce} = 1.7 \cdot 10^{23} \frac{(kT_e)^{3/2}}{n_e \ln \Lambda} \qquad \ln \Lambda = \text{Coulomb logarithm}$$

$$t_{ci} = \left(\frac{m_i}{m_e}\right)^{1/2} \cdot t_{ce} \qquad (12)$$

$$t_{eq} = 0.516 \frac{m_i}{m_e} \cdot t_{ce}$$

The set of coupled differential equations (5) to (8) has been solved numerically by a computer program for various realistic values of A(o)and A_R.

Before discussing these results a rough estimate of the importance of the different terms in equations (6) and (7) and of the effect of superimposing an axial magnetic field will be made. For this purpose a plasma with typical values of electron density $n_e(o) = 1 \times 10^{13} cm^{-3}$, electron temperature $T_e(o) = 1$ eV and gas pressure 3×10^{-3} Torr H_2 (corresponding to $n_n(O) = 1 \times 10^{14} cm^{-3}$) is considered. Then the equipartition time t_{eq} is about 3.5 µsec for electrons and H^+ (t_{eq} proportional to n_e^{-1}) indicating that the two temperatures will relax to a mean temperature after a few microseconds. With respect to heat conduction by electrons (the heat conduction by ions is about 2o times smaller for $T_e = T_i$) it turns out that without axial magnetic field the time

$$\tau = \frac{R^2}{5.75 \cdot D} \qquad \text{with} \quad D = \frac{e}{k\, n_e}$$

in which the electron temperature on the axis of our discharge tube (R = 7 cm) drops to 1/e of its initial value is about 1 μsec, which is a rather fast energy loss (τ increases proportional to R^2 and, for $B_o = 0$, to n_e).

We therefore now turn to the question of how heat conduction and ambipolar diffusion are reduced by an axial magnetic field B_o. To find out how large B_o has to be in order to have a noticeable effect, we set the expressions containing B_o in the denominator of equations (9) and (10) equal to 1. From equation (10) we find

$$(B_o)_{\text{heat cond.}} \geqslant 2.8 \times 10^{-7} \frac{n_e \ln\Lambda}{T_e^{3/2}}$$

$$\approx 20 \text{ Gauss for } n_e = 10^{13}\text{cm}^{-3} \text{ and } T_e = 1 \text{ eV},$$

which shows that a very small magnetic field of the order 100 Gauss should be sufficient to reduce the heat conduction considerably. Similarly we get for the ambipolar diffusion from equation (9)

$$(B_o)_{\text{amb.diff}} \geqslant 1.1 \times 10^{16} m_i^{1/2}\, p(\text{Torr})$$

$$\approx 40 \text{ Gauss for } p = 3 \text{ mtorr and } m_i = m_{H^+},$$

which is of the same order as $(B_o)_{\text{heat cond.}}$.
In an actual experiment in both cases axial losses may become the limiting effects if the radial losses are reduced by superposition of an axial magnetic field.

The effect of an axial magnetic field on the ambipolar diffusion has been checked experimentally and is in very good agreement with the above considerations. Figure 5 shows the decay times for $B_o = 0$, 220 and 285 G in hydrogen plasmas

at 3 and 10 mtorr filling pressure. Figure 8 shows the time in which the electron density drops to 1/e of its maximum value, $n_{e\ max}$, as a function of the amplitude of the axial magnetic field B_o for 3 mtorr filling pressure. This and similar results for 6 and 10 mtorr show that magnetic fields of a few tens of gauss are sufficient to reduce the diffusion time and that for a fixed value of B_o the change in diffusion time is larger at lower filling pressures. The experimental result that the decay time could not be extended by axial magnetic fields beyond a certain value (approximately 35 μsec at 3 mtorr H_2 and 14 μsec at 10 mtorr H_2) indicates that under those conditions the decay of electron density was governed by processes other than radial diffusion. The most likely processes are axial losses due to the short length of the solenoid.

Figures 9 and 10 show typical numerical results of the time evolution of density n, electron temperature T_e and ion temperature T_i in a plasma described by eqs.5 to 12. In these calculations the neutral gas temperature T_n which appears in eq. 9 has been set equal to 0.026 eV ($\cong 300^oK$), while the density and temperature at the plasma boundary have been assumed to be $n_R = 1 \times 10^{11} cm^{-3}$ and $T_{eR} = T_{iR} = 0.1$ eV. Varying n_R between 1×10^{10} and $1 \times 10^{12} cm^{-3}$ and T_{eR} between 0.025 and 0.4 eV did not noticeably change the results except near the boundary. The results plotted in Figures 9 and 10 are for the conditions listed in table II that resemble those of our preionization experiment. In the case of hydrogen the plasma was assumed to be composed of electrons and H^+ ions, in the case of argon of electrons and Ar^+ ions.

From the numerical calculations the following conclusions can be drawn for our test gas.

Hydrogen:

a) The time for energy equipartition between electrons at 2 eV and H^+ ions at 0.1 eV is a few μsec. This suggests starting the calculations at higher densities with $T_e(o) = T_i(o) \approx 1$ eV (Figure 9d).

b) In a tube of 7 cm radius or larger the decay of density due to ambipolar diffusion becomes appreciable only for $n(o) > 5 \times 10^{13} cm^{-3}$ (Figure 9c) at a filling pressure of 10 mTorr H_2, but is substantial (with $B_o = 0$) for all our conditions at filling pressures of a few mTorr H_2 (Figure 9e).

c) The radial diffusion can substantially be reduced by an axial magnetic field B_o of order 100 gauss (Figure 9f) which at the same time diminishes the radial heat conduction losses.

d) In a vessel three times larger in diameter than that used here, it should be possible to make the equipartition times of the same order or shorter than the dominant loss mechanisms (Figure 9b), since the characteristic times for radial ambipolar diffusion and heat conduction scale as R^2.

Noble gases (e.g. argon):

a) The energy equipartition time is proportional to the ion mass (c.f. eq.12) and in the case of argon is about 300 μsec for our typical conditions (Figure 10 b).

b) During times of the order of the energy equipartition time the decay of density in a tube of 20 cm radius is negligible. The same is true for the radial heat conduction losses if an axial magnetic field B_o of order 100 gauss is present (Figure 10 b).

V. Conclusions

It has been shown that the photoionization technique described above can be used to produce highly ionized, clean, radially homogeneous plasmas suitable for collision-free shock studies (c.f.reference 3). With a double ended source the test gas is also relatively homogeneous in axial direction, the electron density being smallest in the median plane and increasing towards each light source. Axial diffusion and conduction will tend to flatten this distribution.

With noble gases the products are singly charged ions and electrons, and the initially cold ions become heated to around 1 eV through equipartitioning of energy with the electrons. When hydrogen is used, the evolution of the plasma is more complicated, and the initial measurements of T_e, n, and composition are being continued in order to obtain a more complete understanding.

For its application to collision-free shock studies it is an interesting feature of this preionization method that values of T_e/T_i ranging from 1 to about 2o can be selected in the photoionized plasma by waiting an appropriate time after firing the light source.

Acknowledgements

We wish to thank Dr.G. Hofmann for his substantial help in developing the experimental apparatus in the early stages of the work and Messrs. H. Finkelmeyer, A. Gattinger, H. Niedermeyer, W. Stegmann, and K.H. Steuer for their help with the measurements.

We are grateful to Dr. R. Gorenflo and Mr. J. Steuerwald for developing a computer program and carrying out the numerical calculations.

Appendix I

Estimate of Temperature and Density in the Xenon Pinch Column

In order to calculate the emission of radiation from the Xenon source, its temperature and density must be known. These quantities can be estimated roughly from the pinch dynamics, as observed by an image converter streak camera. Specifically, from the measured implosion speed the thermodynamic properties behind the incident shock can be calculated using plane shock jump conditions and neglecting the effects of cylindrical convergence. When the shock wave reflects from the axis, the gas at the center comes to rest with further heating and compression. The reflected outgoing shock reflects again from the incoming magnetic piston; in this way a series of progressively weaker compression waves traverses the plasma, leading in the final stages to a reversible approach to quasi-equilibrium between the confining magnetic field and the plasma pressure.

The calculation presented below ignores the variation in filling density along the axis, which is not precisely known, and considers only the heating due to the incident and first reflected shock waves. Ohmic heating is omitted, as is the loss of energy by radiation.

Assume a shock wave propagating with a Mach number M_1 into room temperature Xenon at a pressure p_1. The conservation eqns., in shock-fixed coordinates are

$$\begin{aligned} \rho_1 u_1 &= \rho_2 u_2 \\ p_1 + \rho_1 u_1^2 &= p_2 + \rho_2 u_2^2 \\ h_1 + \tfrac{1}{2} u_1^2 &= h_2 + \tfrac{1}{2} u_2^2 \end{aligned} \qquad (1)$$

For an ideal gas, $h = \frac{\gamma}{\gamma-1}\frac{p}{\rho}$, and the ratios ρ_2/ρ_1, p_2/p_1, and T_2/T_1 depend on the single parameter

$$M_1^2 = \frac{u_1^2}{\gamma (p_1/\rho_1)}$$

For an ionizing gas, the simple eqn. of state must be replaced by $h = h(p, \rho)$ or an equivalent thermodynamic description. In this case the temperature, pressure, and density ratios depend on both M_1 and p_1. The density ratio remains bounded for large M, but can reach values of 10 to 15 instead of 4, as for an ideal monatomic gas. The conservation laws can be put into the form

$$\begin{aligned} \frac{p_2}{p_1} &= 1 + \gamma_1 M_1^2 \left(1 - \frac{1}{\eta}\right) \\ \frac{h_2}{h_1} &= 1 + \frac{\gamma-1}{2} M_1^2 \left(1 - \frac{1}{\eta^2}\right) \qquad (2) \\ \frac{u_p}{a_1} &= M_1 \left(1 - \frac{1}{\eta}\right) \end{aligned}$$

where $\eta = \frac{\rho_2}{\rho_1}$ and $u_p = |u_1 - u_2|$

The total enthalpy for a mixture of multiply ionized species is

$$\rho h = \rho_n h_n + \sum_{i=1}^{l} \rho_i h_i + \rho_e h_e \qquad (3)$$

when h denotes specific enthalpy, the subscripts n, i refer to neutral and i times ionized atoms respectively, and e denotes electron properties.

Assuming perfect gas behavior for the individual species and temperature equilibration between species, then

$$h_n = \frac{5}{2}\frac{k}{m_n}T$$
$$h_i = \frac{5}{2}\frac{k}{m_i}T + h_o^i \qquad i = 1, 2, \ldots \ell \qquad (4)$$
$$h_e = \frac{5}{2}\frac{k}{m_e}T$$

where $h_o^i = \frac{1}{m_i}\sum_{q=1}^{i}\phi_q$

ϕ_q = ionization energy of q^{th} level

h_o^i is a measure of the binding energy of the i^{th} species. These relations ignore the energy of bound excited electrons.

Letting $n \equiv n_n + \sum_{i=1}^{\ell} n_i$,
and assuming for all ionic species that $m \equiv m_n \approx m_i$,
then $\rho \approx nm$ and equation (3) simplifies to

$$h = \frac{5}{2}\frac{kT}{m}\left(1 + \frac{n_e}{n}\right) + \frac{1}{\rho}\sum_{j=i}^{\ell}\sum_{i=1}^{\ell} n_j \phi_i \qquad (5)$$

In order to calculate the required number densities, one can use the Saha equation[18]. This completes a method by which to determine the temperature and ionization state of the pinched gas.

The iterative computational procedure is as follows:

1) Using the known imploding shock speed, guess a value for $\eta^{(o)}$ and calculate $h_2^{(o)}/h_1$ by equation (2). h_1 is known from initial conditions.

2) Guess a temperature and a value of n_e and use the equation of state (3) to calculate the desired number densities, n_i and n_n.

3) Calculate h_2 from equation (5) using the results of step 2).

4) Compare with step 1) and iterate. The calculation converges repidly due to the weak dependence of h and p on η.

Numverical calculations have been carried out according to the above procedure for the Xenon light source for typical cases. The assumed shock speed was 2.3cm/μsec (M_1 = 130), in accordance with the streak photographs, and the initial filling pressure was 1 torr. The calculations could only be carried to T = 40,000°K because of the parameter range of reference (18). At this temperature h_2 is about one third of the value required by the conservation law (for M_1 = 130, η = 10, γ = 5/3). If one extrapolates the calculated values of h_2 beyond 40,000°K it appears that the equilibrium temperature behind the shock should be roughly 60,000 to 70,000°K; most of the energy has gone into ionization and relatively little into thermal motion. (An ideal gas calculation, ignoring ionization, gives $T_2 = 1.54 \times 10^6$.) A rough etstimate, based on the assumption that each stage of ionization is complete before the next one is begun, indicates that the gas should be about five times ionized.

The calculation just described gives conditions behind the incident shock. The kinetic energy density behind the incident shock, $\frac{1}{2} u_p^2$, can be deduced from equations (2) to be about equal to h_2. Thus, when the shock reflects, the enthalpy approximately doubles. It can be shown that the enthalpy behind the reflected shock (h_3) can be written as

$$\frac{h_3}{h_2} = \frac{2(\eta\sigma - 1)}{(\eta+1)(\sigma-1)},$$

where σ is the density ratio across the reflected shock,

which for our conditions is approximately equal to η. Thus, $h_3 / h_2 \approx 2$, as stated above. Extrapolations of the calculated values of h_2 show that reflection of the shock should produce a temperature increase of about 1 e.v. with a corresponding increase in Z of about 1.

We acknowledge the help of Mr. Noel Amherd in carrying out these calculations.

Appendix II

Comparison of ionizing efficiency of the xenon and hydrogen pinches

In order to compare the expected efficiencies of the hydrogen and xenon pinches in ionizing a hydrogen gas, we first calculate the emission coefficient ε for both plasmas at a density of $10^{18}\,cm^{-3}$ and the temperatures estimated in Appendix I (about 50 eV for hydrogen and a few eV for xenon).

For a xenon plasma under these conditions the largest contribution to the emission coefficient comes from radiative recombination. It can be calculated from eq. 5-36 of reference 20) which, with the assumptions stated on p. 12 , reduces to

$$\varepsilon_{Xe,z} \sim \frac{z^4}{(kT)^{3/2}} \left[\sum_{n=n_{min}}^{2} \frac{1}{n^3} \exp\left(\frac{E_\infty^{Xe,z-1} - \langle E_n \rangle_\ell^{Xe,z-1}}{kT} \right) \right]$$

$$\cdot N_e N^{Xe,z} \exp\left(\frac{-\Delta E_\infty^{Xe,z-1} - h\nu}{kT} \right)$$

$$= \varepsilon'_{Xe,z} \cdot \frac{N_e}{(kT)^{3/2}} \exp\left(- \frac{h\nu}{kT} \right)$$

All symbols have the same meaning as in reference 20). $\langle E_n \rangle_\ell^{Xe,z}$ is the mean value of $E_{n,\ell}^{Xe,z}$ with respect to ℓ . Its numerical values have been taken from reference 28). For the second energy levels of Xe V, Xe VI and Xe VII extrapolated values have been used. The total ion densities on the different ionization stages, $N^{Xe,z}$, were calculated using tabulated values of the Saha equation[18].

In the case of a hydrogen plasma of the above-mentioned density and temperature the main contribution to the emitted radiation comes from bremsstrahlung and correspondingly we get

$$\varepsilon'_H \sim \frac{kT}{2E_H} \exp\left(-\frac{\Delta E_\infty^{z-1}}{kT}\right) \exp\left(\frac{z^2 E_H}{n_1^2 kT}\right) N^H$$

Calculation of the radiation emitted by a 1 cm column of xenon at a few eV and hydrogen at 50 eV shows that in both cases the plasma is optically thin at a density of 10^{18} cm^{-3}. The relative degree of ionization produced per unit time by the two light sources can therefore be calculated from

$$\frac{\partial \alpha}{\partial t} \sim \int_{\nu_0}^{\infty} \frac{\sigma_{ion}\, \varepsilon\, d\nu}{h\nu}$$

With $\sigma_{ion} \sim \nu^{-3}$ one gets for the relative ionization rates

$$\frac{\partial \alpha_H}{\partial t} \sim \frac{\varepsilon'_H(kT)}{(kT)^{9/2}} \int_{h\nu_0/kT}^{\infty} \frac{e^{-x}}{x^4}\, dx$$

$$\frac{\partial \alpha_{Xe}}{\partial t} \sim \sum_z \frac{\varepsilon'_{Xe}(z,kT)}{(kT)^{9/2}} \int_{h\nu_{a,z}/kT}^{h\nu_{b,z}/kT} \frac{e^{-x}}{x^4}\, dx$$

where $x = h\nu/kT$, ν_0 = lower frequency limit for photoionization of hydrogen and $\nu_{a,z}$, $\nu_{b,z}$ are the frequency limits within which the emission coefficients are constant. The calculated ionization rates are plotted in figure 7 and show that under the assumed conditions the ionization rates produced by the xenon pinch are roughly two orders of magnitude higher than those with the hydrogen pinch. This is in qualitative agreement with the experimental results although the experiments show a smaller difference in ionization rates.

References

1 J.W.M.Paul et al., Nature 2o8, 135 (1965)

2 F.Y.Sorrell, G.C.Vlases, E.A.Crawford, Proceedings APS Topical Conference on High Density Pulsed Plasmas, Los Alamos (1967), Report LA-377o, Los Alamos (1967)

3 R.Chodura, M.Keilhacker, M.Kornherr and H.Niedermeyer, Plasma Physics and Controlled Nuclear Fusions Research , Vol.I, 81, International Atomic Energy Agency, Vienna (1969)

4 M.Keilhacker, M.Kornherr and K.-H.Steuer, Z.Physik 223, 385 (1969)

5 A.W.De Silva et al., Plasma Physics and Controlled Nuclear Fusion Research, Vol.I,143, International Atomic Energy Agency, Vienna (1969)

6 E.Hintz, Plasma Physics and Controlled Nuclear Fusion Research, Vol.I,69, International Atomic Energy Agency, Vienna (1969)

7 W. Köppendörfer, Report IPP 1/79,Institut für Plasmaphysik, Garching bei München (1968)

8 G.Hofmann,J.Quant.Spect.Rad.Transfer 8, 729 (1968)

9 See E.Fünfer,Proceedings APS Topocal Conference on High Density Pulsed Plasmas, Los Alamos (1967), Report LA-377o, Los Alamos (1967)

lo F.Pecorella and G.Vlases, Physics Letters 28A, 616 (1969).

11 G.Marr, Photoionization Processes in Gases, Academic Press, New York (1967)

12 H.Brinkschulte et al.,Z.f.angew.Physik 25, lo9 (1968)

13 J.R.Barker, J.Sci.Inst.26, 273 (1949)

14 K.-H.Steuer, Report IPP 1/94, Institut für Plasmaphysik, Garching bei München (1969)

15 H.Niedermeyer, Report IPP 1/66, Institut für Plasmaphysik, Garching bei München(1967)

16 A.Gattinger, Institut für Plasmaphysik,Garching bei München, (private communication)

17 See for example, H.W.Liepmann and A.Roshko, Elements of Gasdynamics, J.W.Wiley and Sons, New York (1957)

18 H.W.Drawin and P.Felenbok, Data for Plasmas in Local Thermodynamic Equilibrium, Gauthier-Villars,Paris (1965)

19 G.Hofmann and F.Pecorella, J.Quant.Spect.Rad.Transfer 8, 735 (1968)

2o H.R.Griem, Plasma Spectroscopy, McGraw-Hill, New York (1964)

21 See Culham Laboratory Progress Report, CLM-PR lo, pg. 96 (1967)

22 E.Schönheit, Z.f.Naturf. 15a, 841 (196o)

23 D.R.Bates, A.E.Kingston, and R.W.P.McWhirter, Proc.Roy. Soc. A267, 297 (1962)

24 H.S.Carslaw and J.C.Jaeger, Conduction of Heat in Solids, 2nd ed., Oxford University Press (1959)

25 S.C.Brown, Introduction to Electrical Discharges in Gases, J.Wiley and Sons, New York (1966)

26 D.Düchs, Report IPP 1/14, Institut für Plasmaphysik, Garching bei München (1963)

27 L.Spitzer, Physics of Fully Ionized Gases, 2nd ed., John Wiley and Sons, New York (1965)

28 Ch.E.Moore, Atomic Energy Levels, Vol. III, Circular of the National Bureau of Standards 467 (1958)

29 M.Keilhacker, Report IPP 1/106, Institut für Plasmaphysik, Garching bei München (1970)

Table I

Degree of ionization (%) attainable in various gases at center of 15o cm long test chamber, using xenon as the radiation source.

Gas	Initial Pressure (mtorr)			
	1o	5	3	1
H_2	12.3	16.o	19.2	22
Ar				49
Xe				63

Table II

Initial values for numerical results of Figures 9 and 1O.

Figure:	9a	9b	9c	9d	9e	9f	1oa	1ob
gas	He						Ar	
R(cm)	7	2o	7	7	7	7	2o	2o
p_o(mtorr)	1o	1o	1o	1o	1	1	1	1
$n(0)x10^{-13}(cm^{-3})$	1	1	5	1	1	1	1	1
$T_e(0)$ (eV)	2	2	2	1	2	2	2	2
$T_i(0)$ (eV)	.1	.1	.1	1	.1	.1	.1	.1
B_o(Gauss)	0	0	0	0	0	5o	0	2oo

List of Figures

Figure 9 Calculated time evolution of density n, electron temperature T_e, and ion temperature T_i in a hydrogen plasma cylinder for the initial conditions of table II. The numbers in brackets are the time in μsec.

Figure 10 Calculated time evolution of density n, electron temperature T_e, and ion temperature T_i in an argon plasma cylinder for the initial conditions of table II. The numbers in brackets are the time in μsec.

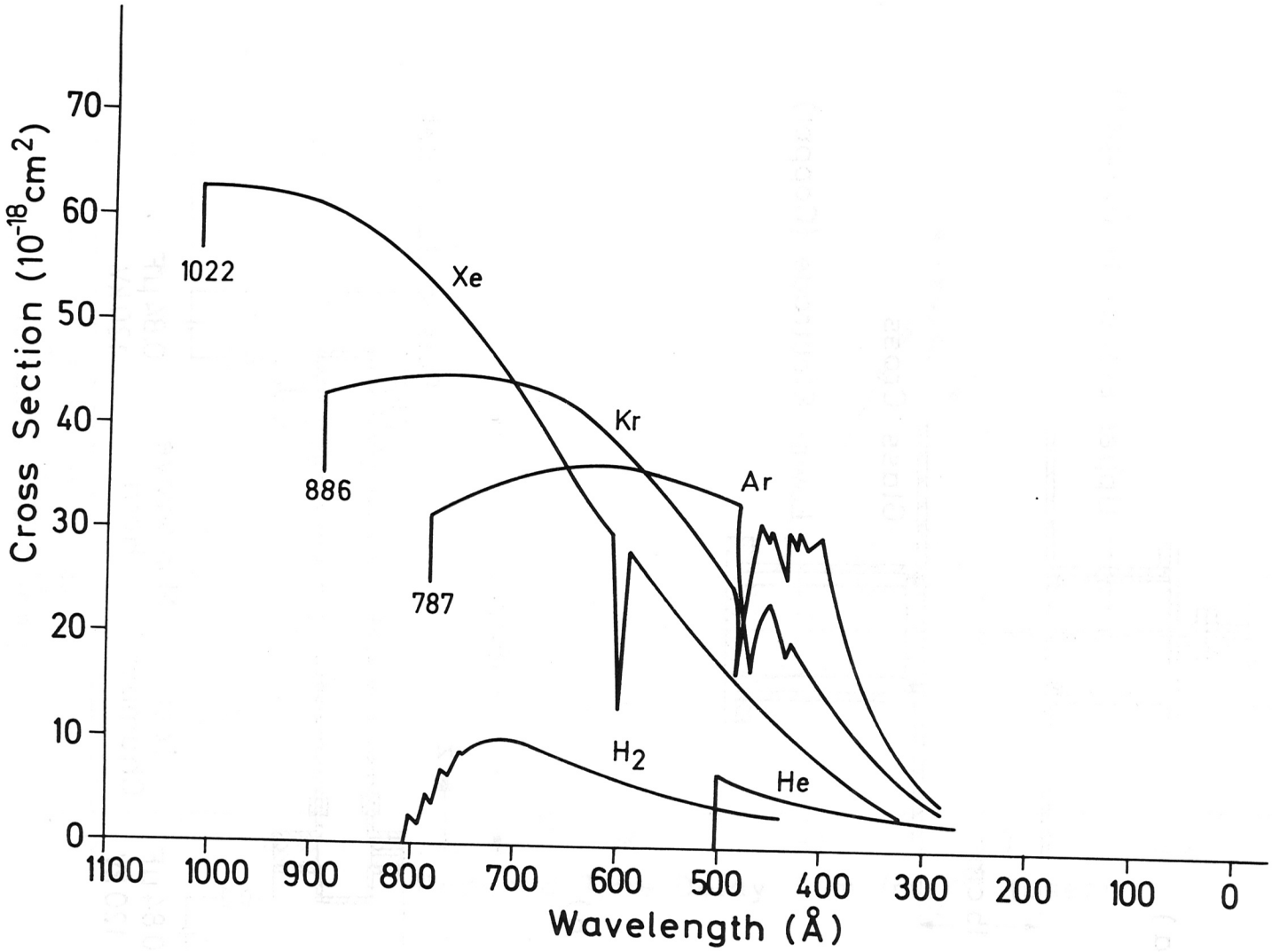

Fig. 1 Photoionization cross sections for H_2 and some noble gases (from Marr (11)).

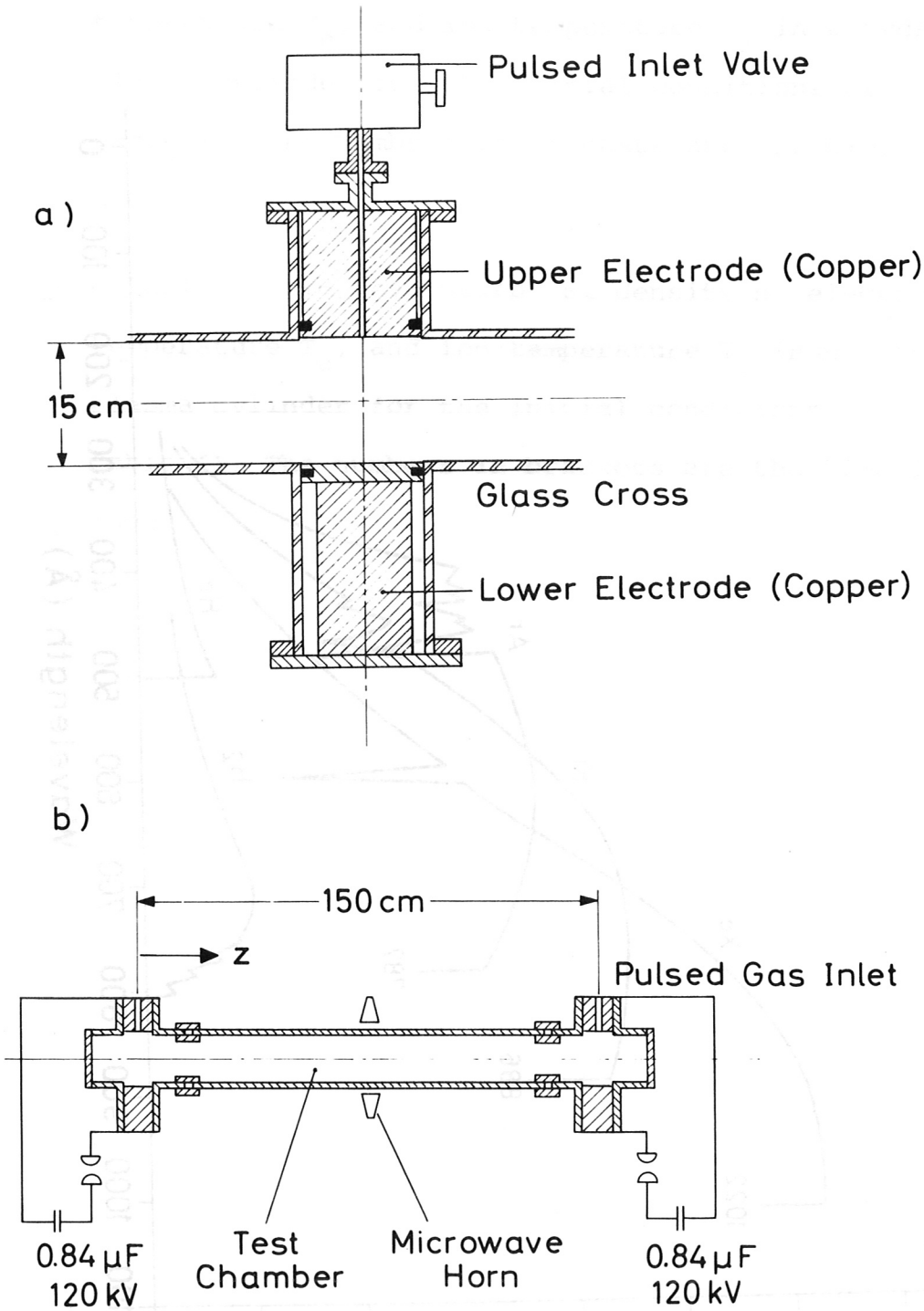

Fig. 2 Schematic diagram of apparatus
(a) Detail of Z-pinch light source
(b) Overall experimental configuration.

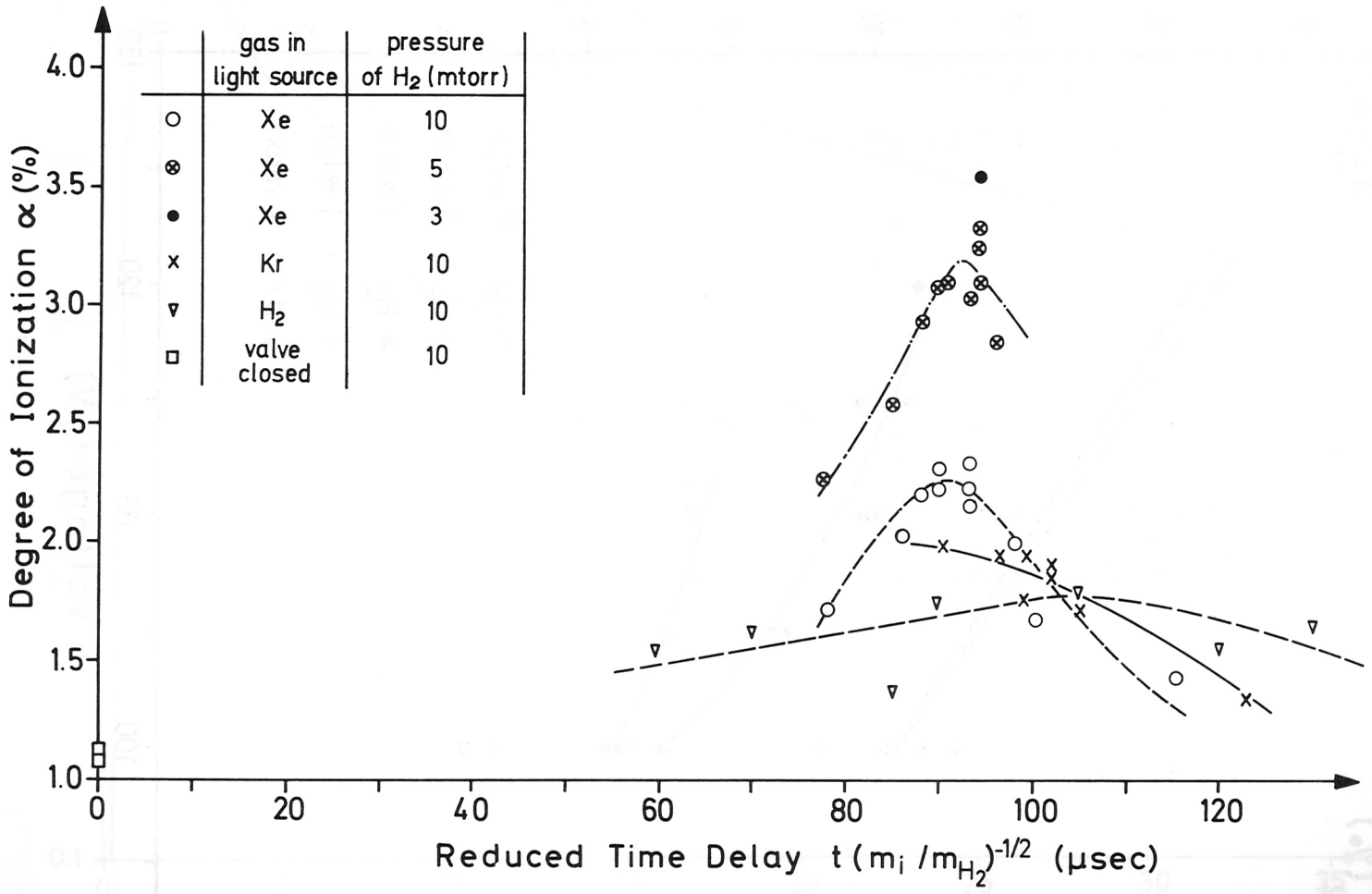

Fig. 3 Variation of α with delay between pulsing of the gas inlet valve and initiation of the pinch current (single-ended light source, z = 100 cm, U_o = 100 kV).

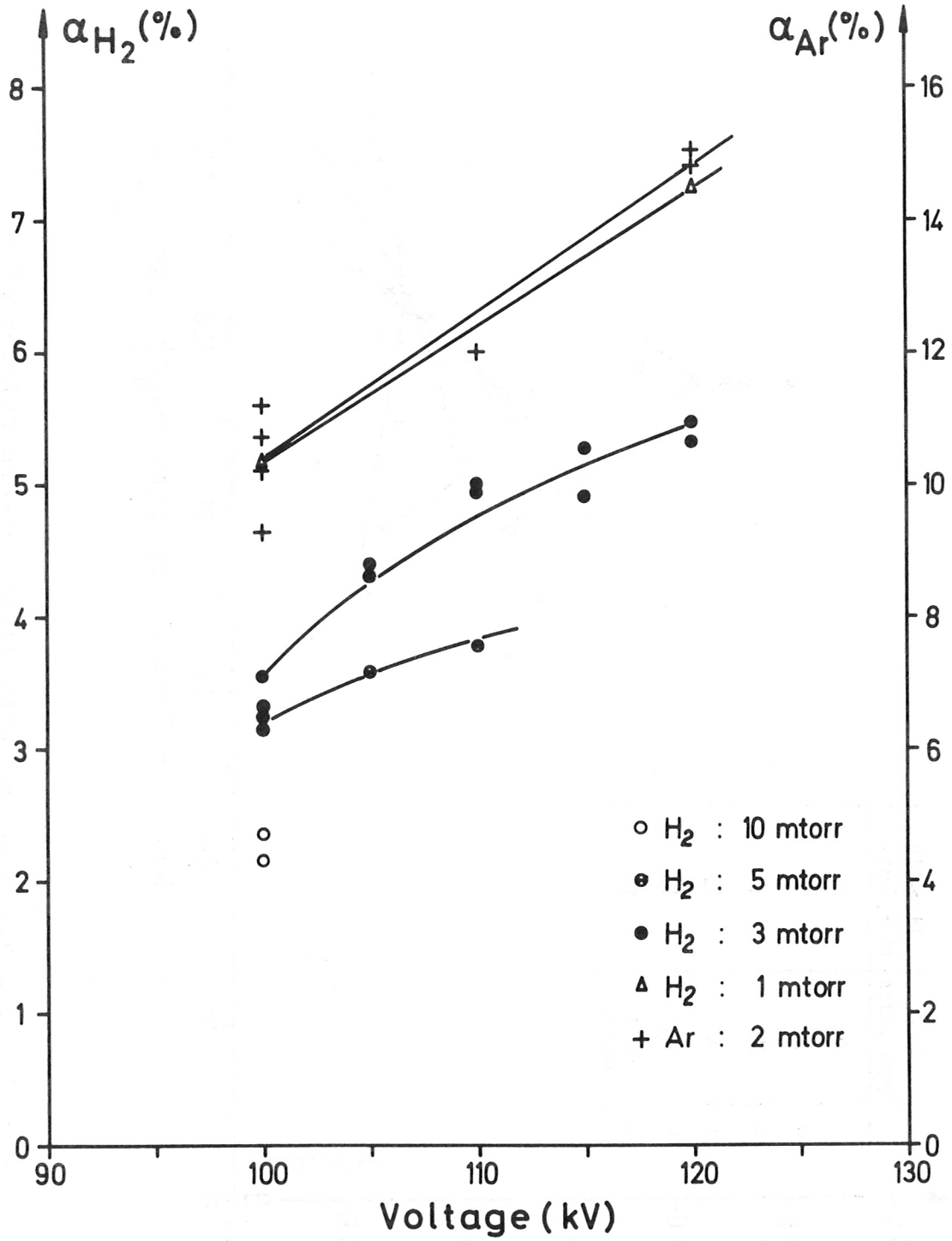

Fig. 4 Variation of α_{max} with capacitor voltage U_o (single-ended source, z = 100 cm).

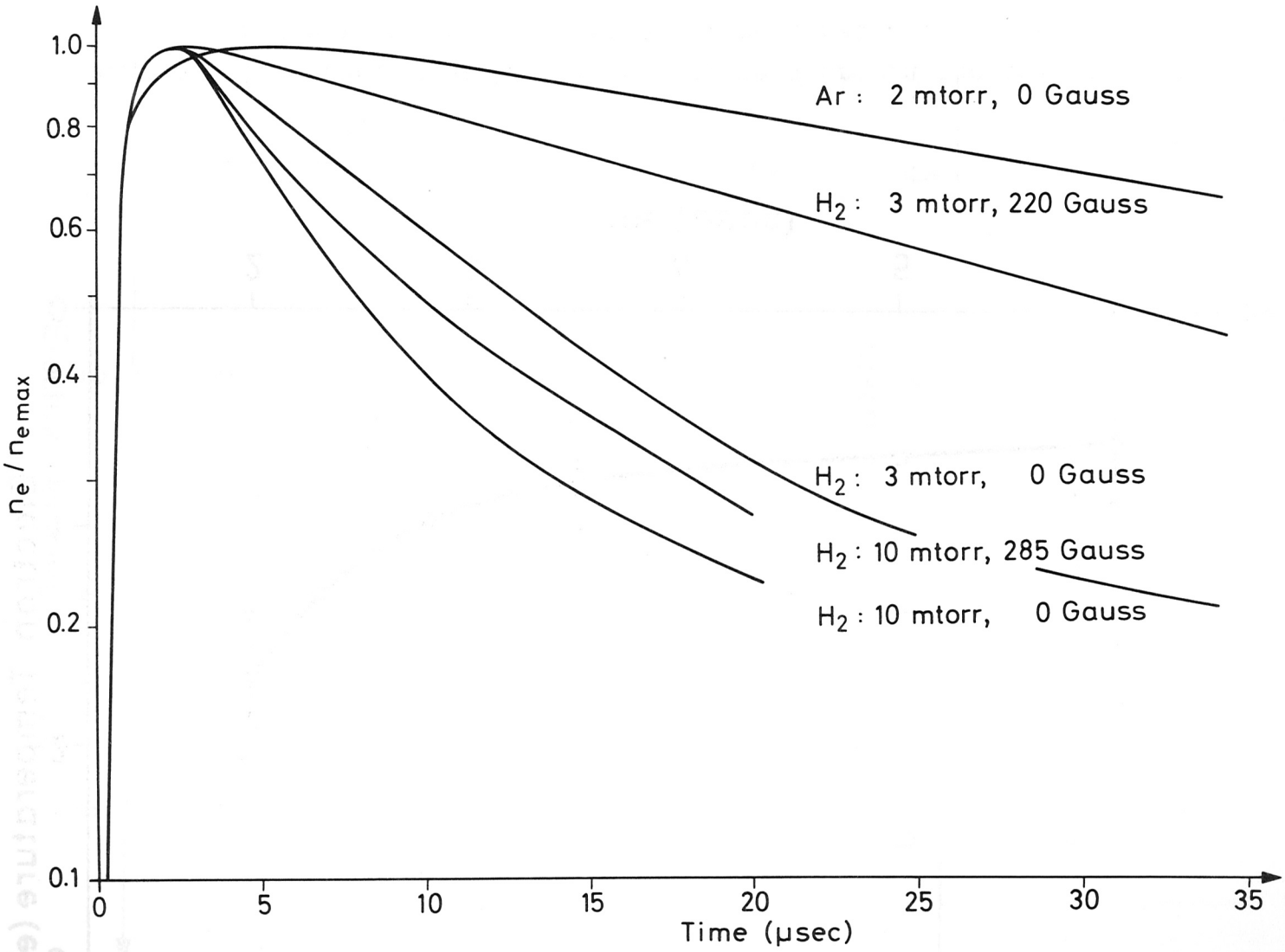

Fig. 5 Time variation of electron density n_e in the test chamber (time is measured with respect to initiation of the pinch current).

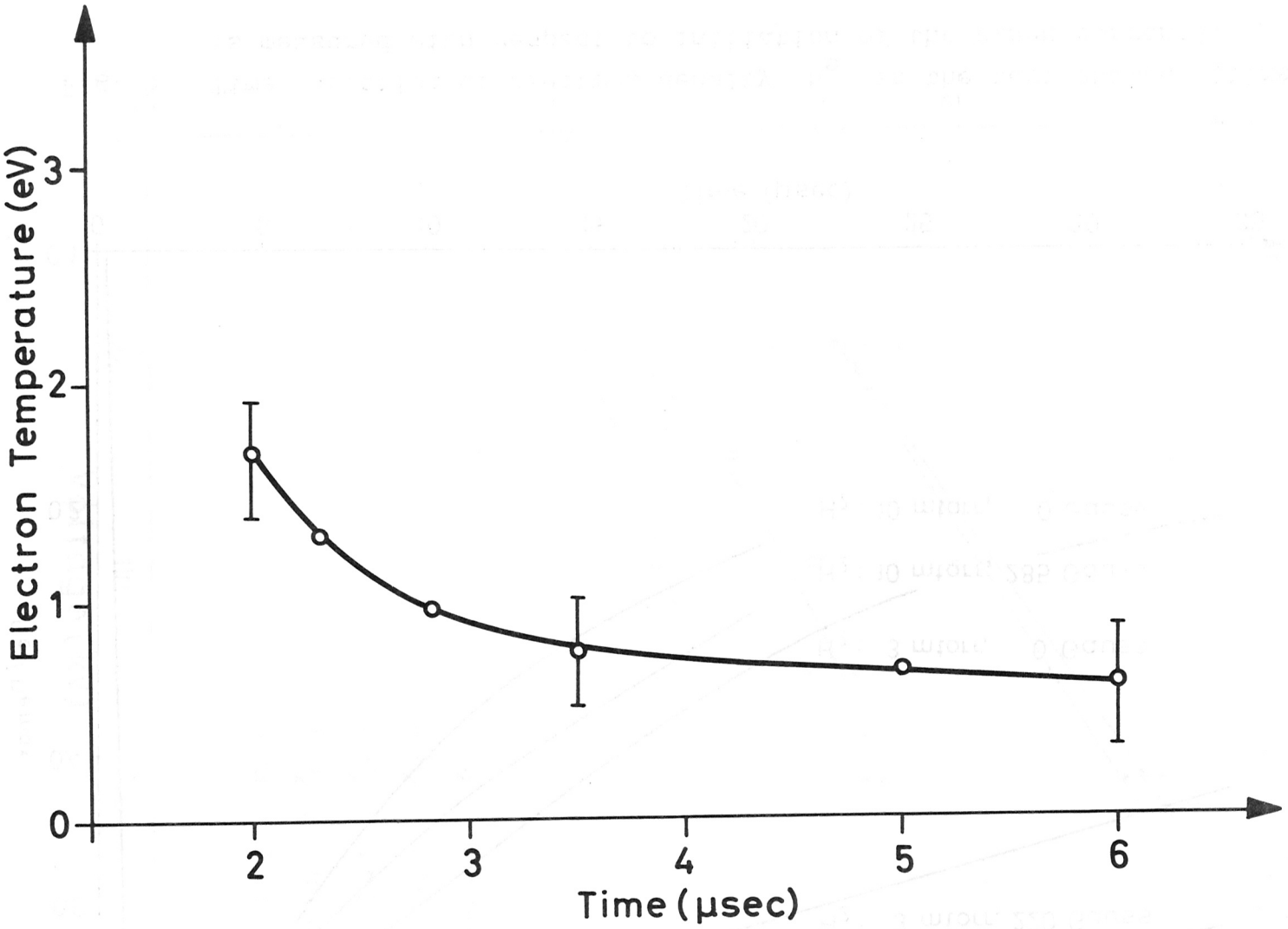

Fig. 6 Time variation of electron temperature in the test chamber for 6 mtorr hydrogen (time is measured with respect to initiation of the pinch current).

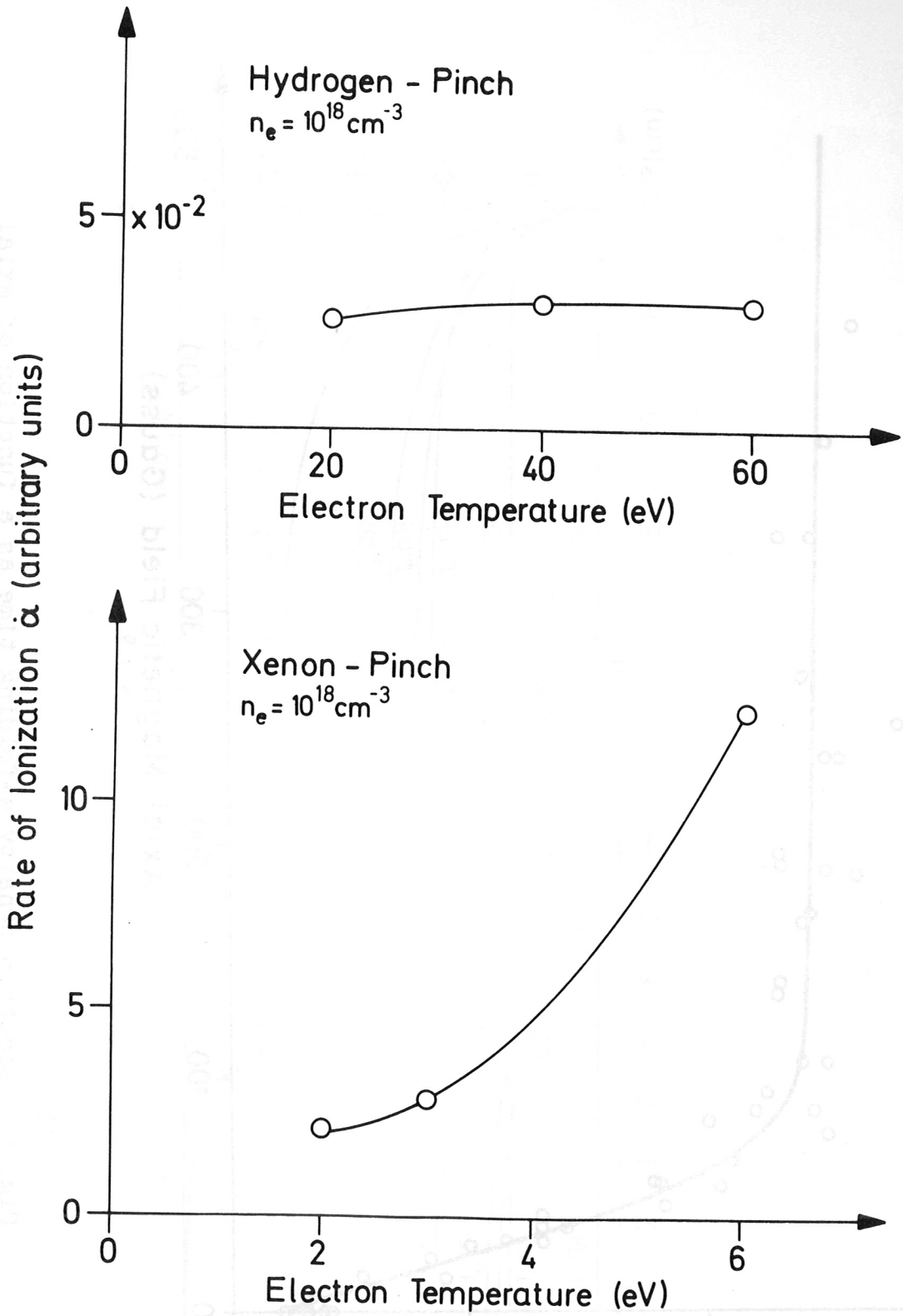

Fig. 7 Relative theoretical ionization rates for Xe and H_2 sources.

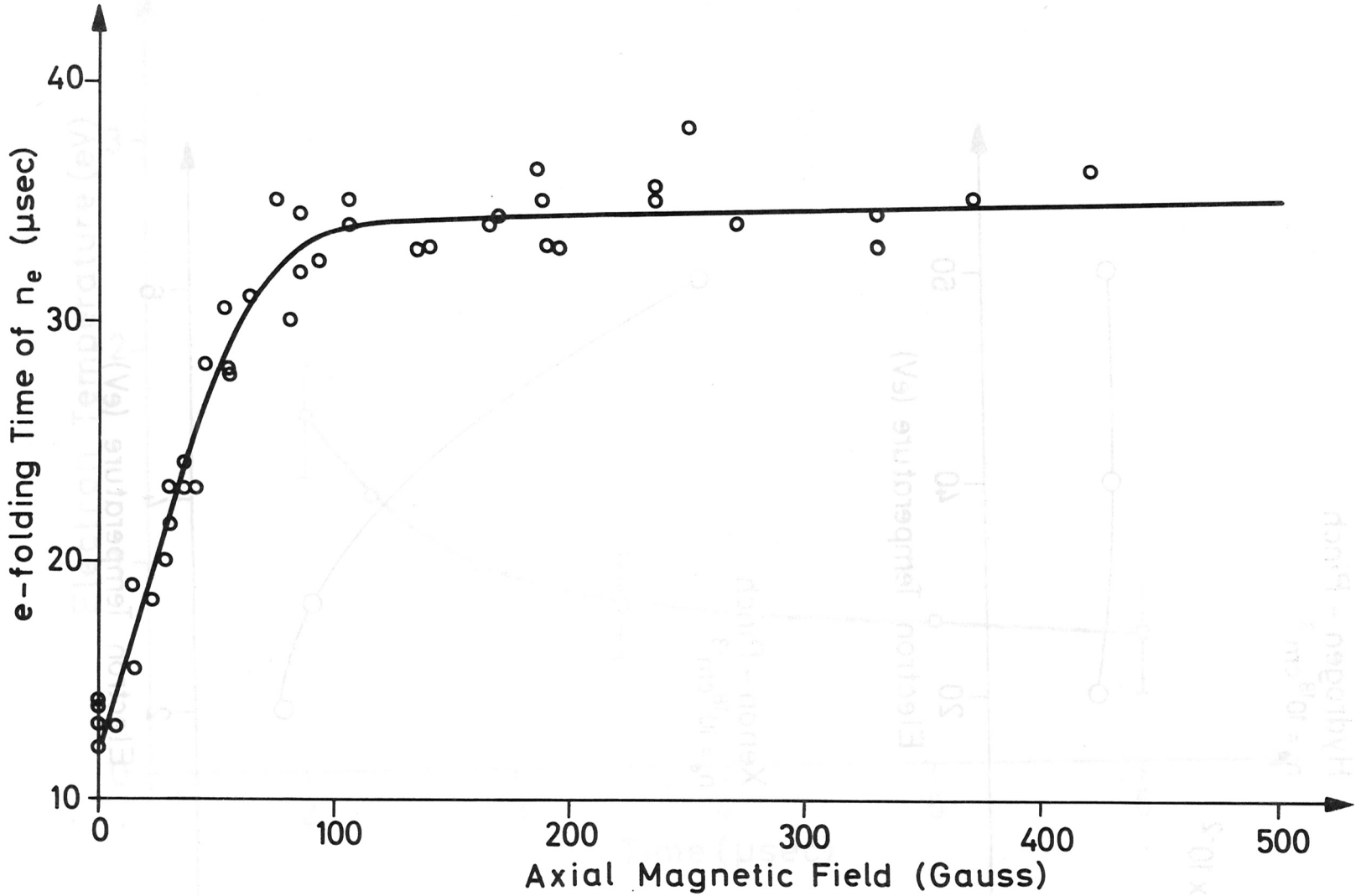

Fig. 8 Electron density e-folding time as a function of axial magnetic field strength for 3 mtorr hydrogen.

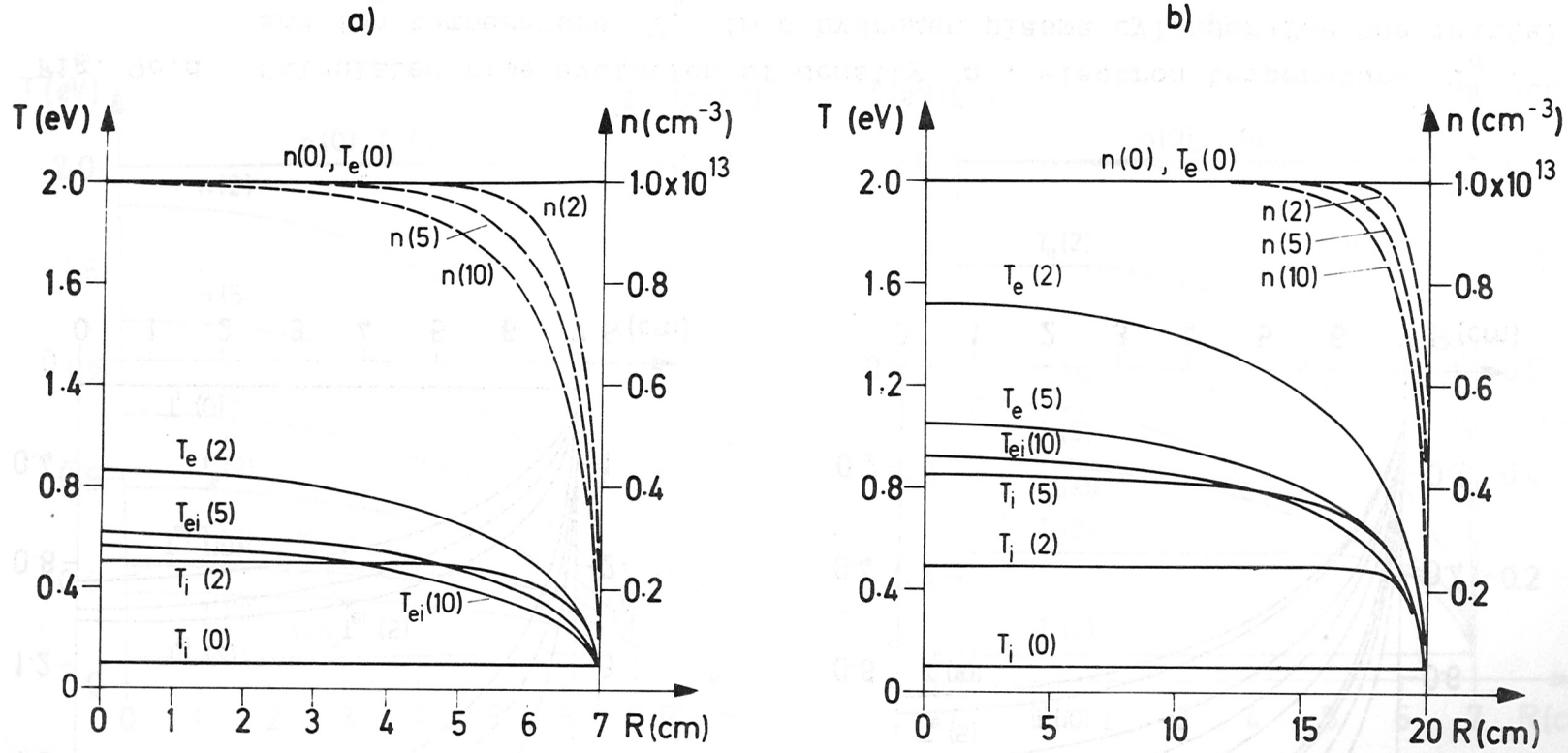

Fig. 9a,b Calculated time evolution of density n , electron temperature T_e , and ion temperature T_i in a hydrogen plasma cylinder for the initial conditions of table II. The numbers in brackets are the time in /usec.

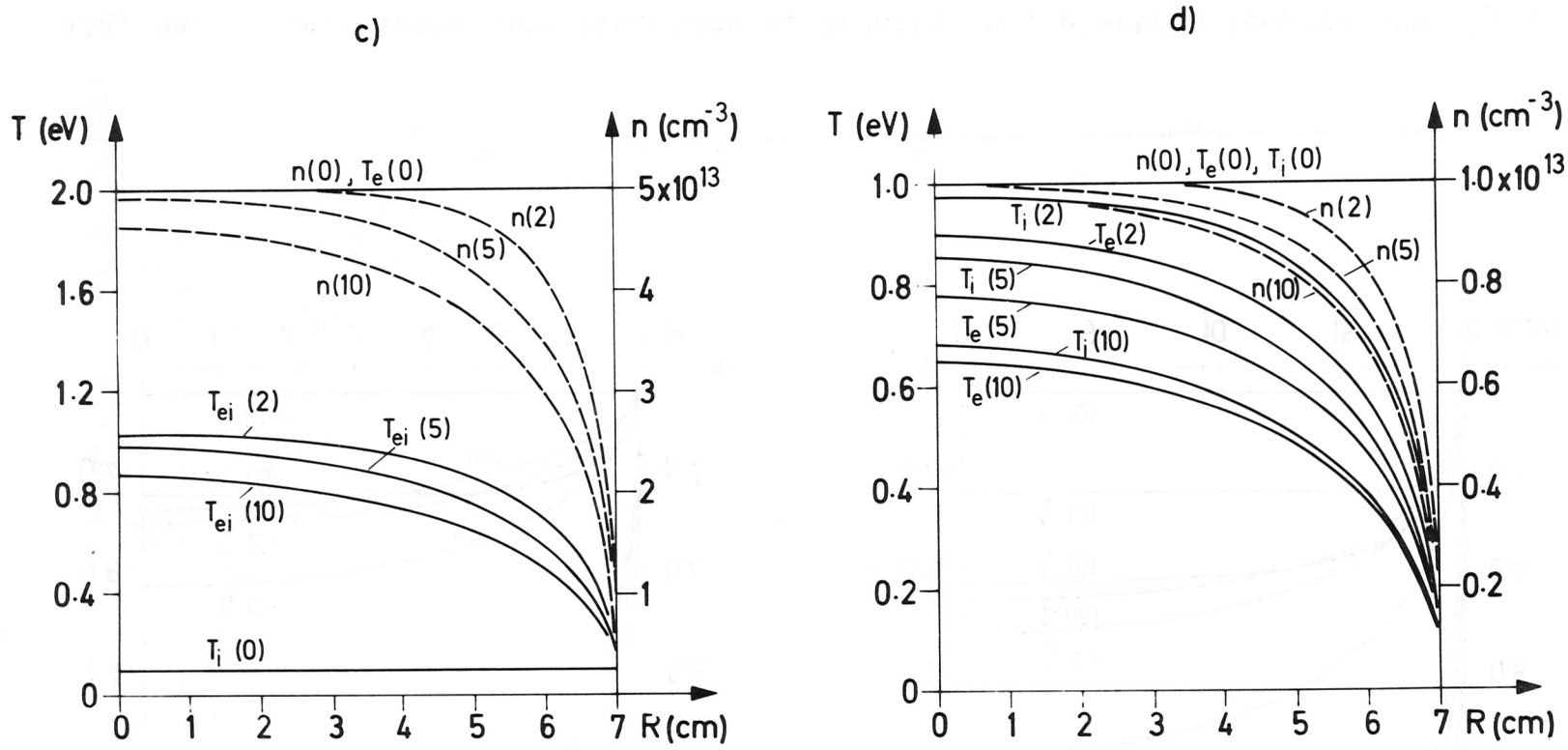

Fig. 9c,d Calculated time evolution of density n , electron temperature T_e , and ion temperature T_i in a hydrogen plasma cylinder for the initial conditions of table II. The numbers in brackets are the time in /usec.

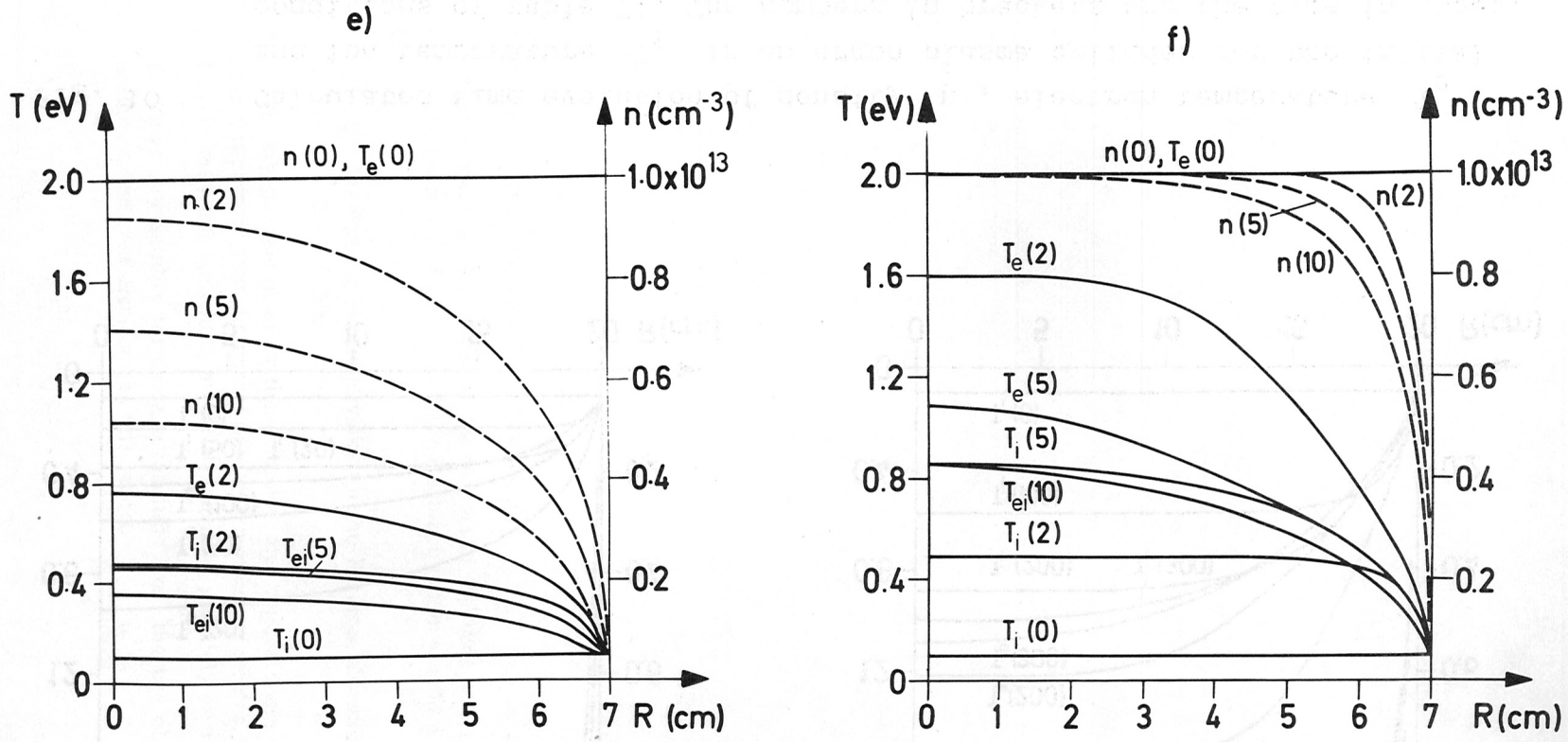

Fig. 9e,f Calculated time evolution of density n , electron temperature T_e , and ion temperature T_i in a hydrogen plasma cylinder for the initial conditions of table II. The numbers in brackets are the time in /usec.

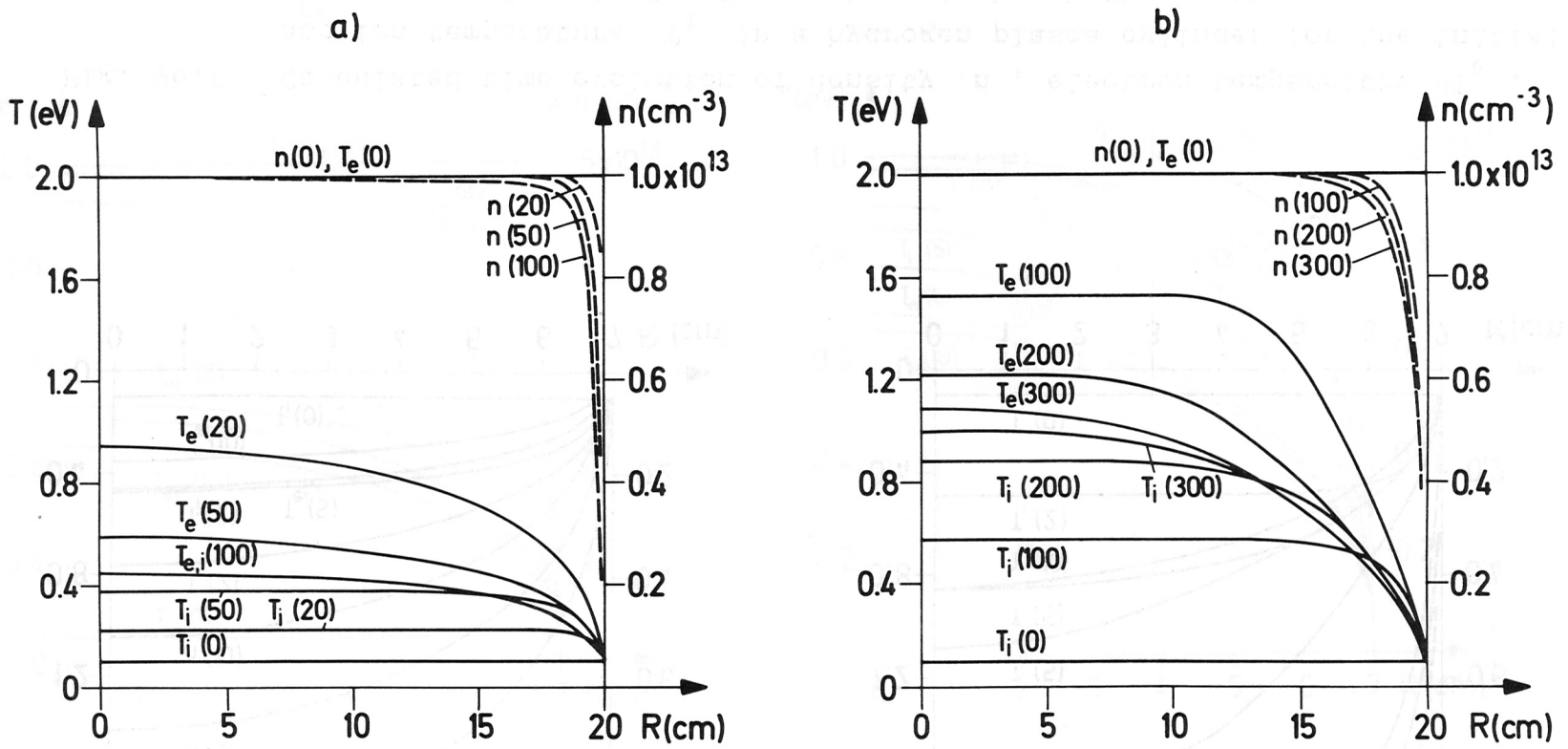

Fig. 10 Calculated time evolution of density n , electron temperature T_e , and ion temperature T_i in an argon plasma cylinder for the initial conditions of table II. The numbers in brackets are the time in /usec.